Geophysical Journal International

Geophys. J. Int. (2011) **187,** 1027–1037 doi: 10.1111/j.1365-246X.2011.05201.x

No direct correlation of mantle flow beneath the North China Craton to the India–Eurasia collision: constraints from new *SKS* wave splitting measurements

Liang Zhao,[1] Tianyu Zheng,[1] Gang Lu[1] and Yinshuang Ai[2]

[1]*State Key Laboratory of Lithospheric Evolution, Institute of Geology and Geophysics, Chinese Academy of Sciences, Beituchengxi Road* 19#, *P.O. Box* 9825, *Beijing* 100029, *China. E-mail: zhaoliang@mail.igcas.ac.cn*

[2]*Key Laboratory of the Earth's Deep Interior, Institute of Geology and Geophysics, Chinese Academy of Sciences, Beituchengxi Road* 19#, *P.O. Box* 9825, *Beijing* 100029, *China*

Accepted 2011 August 23. Received 2011 August 22; in original form 2011 April 28

SUMMARY

The long-range effects of the ongoing India–Eurasia collision and their role in the Cenozoic tectonic evolution of eastern China are not well understood. Here, we investigate deformation beneath the North China Craton and the Qilian Mountain region between the Haiyuan and Kunlun faults, both of which are located immediately to the northeast of the Tibetan Plateau. We present teleseismic shear wave splitting parameters from 299 broad-band stations. These stations provided good spatial coverage in mapping upper-mantle deformation beneath the North China Craton and the Qilian Mountain. The backazimuth dependence of fast directions from stations located within the Qilian Mountain region indicates a complex anisotropy pattern. A multilayer anisotropy and/or anisotropy with a dipping symmetry axis may exist beneath the Qilian Mountain. The overlapping or underthrusting of material evident in anisotropy from this region may be a long-range effect of the India–Eurasia collision. The central North China Craton showed spatially coherent fast directions and the shear wave velocity anomalies within the upper mantle. These patterns suggest horizontal deflection of a regional mantle upwelling, possibly originating from the mantle transition zone. Anisotropy with large delay times was observed in the vicinity of Shanxi rift system. High $\partial \ln V_S / \partial \ln V_P$ values for the upper mantle indicate that anisotropy in this area is enhanced by vertically aligned melt-filled fissures. Our results suggest that the dynamic processes beneath the central North China Craton are not directly related to the India–Eurasia collision.

Key words: Mantle processes; Seismic anisotropy; Asia.

1 INTRODUCTION

The Cenozoic geodynamic evolution of eastern China reflects the complex interplay of the Pacific and the Philippine plates to the east, and the India–Eurasia collision to the southwest. The multidirectional nature of the plate vectors affecting eastern China makes it difficult to determine the primary cause of specific tectonic events in this region. It is widely accepted that the India–Eurasia collision has deformed the upper mantle of the Tibetan Plateau and surrounding regions (e.g. Molnar & Tapponnier 1975; Tapponnier *et al.* 2001; Li *et al.* 2008; Royden *et al.* 2008; Duvall & Clark 2010; Zhang *et al.* 2010), but the effects of the India–Eurasia collision on the upper mantle beneath the North China Craton are not well understood. Some authors (e.g. Wu *et al.* 2005; Li & Li 2007) interpret the Mesozoic to Cenozoic evolution of eastern China primarily in terms of the subduction of the Pacific and Philippine plates, citing temporal and spatial relationships among structural features and magmatism. Other authors (e.g. Liu *et al.* 2004; Tang *et al.* 2006) proposed that Cenozoic rifting and volcanism in eastern China is linked to the India–Eurasia collision, citing large-scale tomographic studies, kinematic modelling and geochemical evidence. Citing the synchronicity of the India–Eurasia collision with the southwest-to-northeast migration of rift activity in China, still, other authors have argued that these rift systems were triggered by convergent tectonism (e.g. Ye 1987). Niu (2005) posits that Cenozoic rifting is due to the migration of asthenospheric material from beneath the western plateaus to eastern China.

Tibet is bounded to the north and east by Phanerozoic Orogens and Precambrian Cratons. Our study area is divided into two regions, the North China Craton and the Qilian Mountain, our study areas, located to the northeast of the Tibetan Plateau (Fig. 1). The WNW–ESE trending northern Qilian Mountain lies between the Haiyuan and Kunlun faults. This area is interpreted to be an Early Paleozoic orogenic belt (e.g. Wang *et al.* 2005) that has been reactivated during the Cenozoic as a strike-slip system (Duvall & Clark 2010). The North China Craton is separated from the Yangtze

© 2011 The Authors
Geophysical Journal International © 2011 RAS

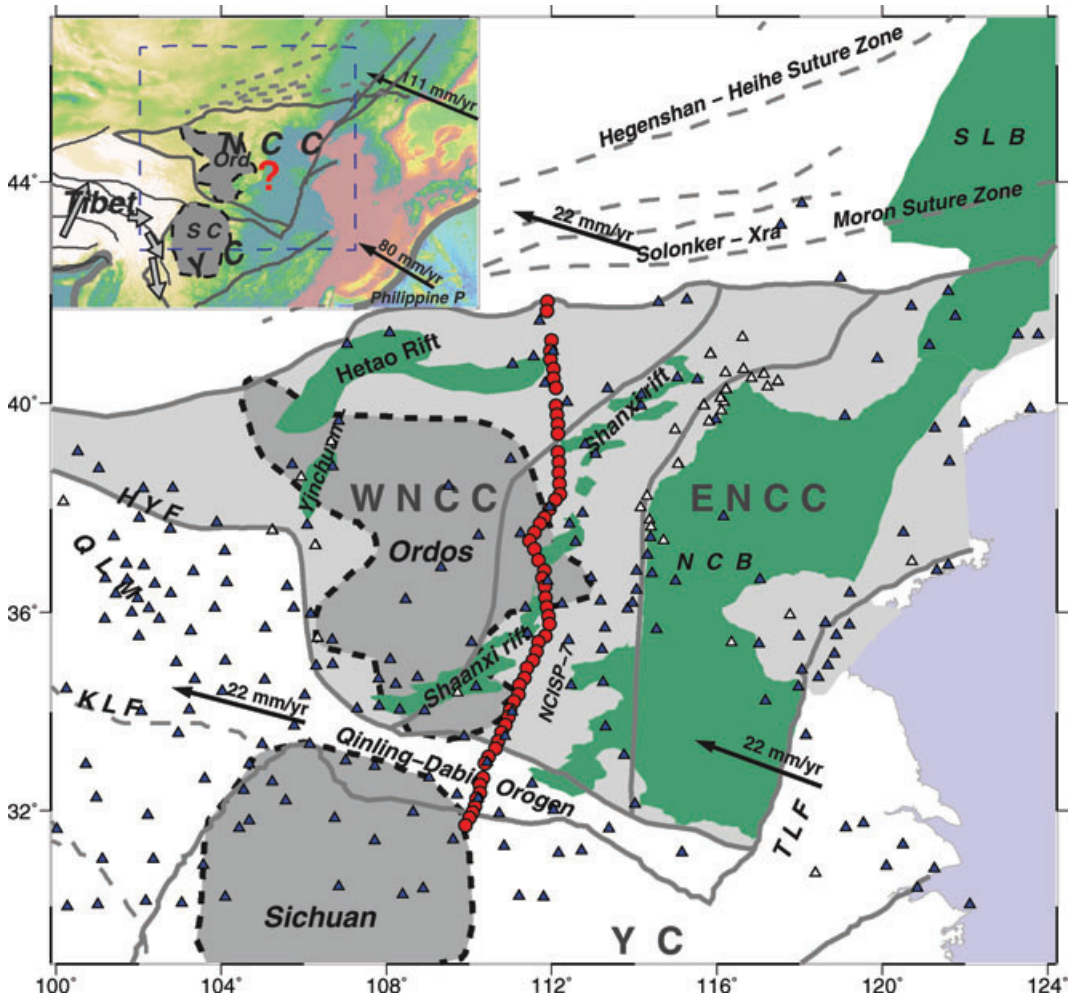

Figure 1. Tectonic map of eastern China showing the seismic networks utilized in this study. Red dots represent North China Interior Structure Project (NCISP) stations, triangles represent Chinese National Seismic Network (CNSN) stations and white triangles represent stations used in previous studies (Zhao & Zheng 2005; Chang *et al.* 2008a; Ma *et al.* 2010). The grey solid lines show the boundaries of major tectonic blocks. Late Mesozoic to Cenozoic rift systems and basins are shaded green. Cratonic zones with high-velocity zones extending to depths of >200 km are shown with dashed lines and dark grey shading. Black arrows represent directions of absolute plate motion (Gripp & Gordon 2002). The inset shows topography overlaid by a simplified tectonic map of the region. Light grey arrows represent the estimated mantle flow channelled from eastern Tibet (e.g. Kind & Yuan 2010). ENCC, eastern NCC; WNCC, western NCC; HYF, Haiyuan Fault; KLF, Kunlun fault; NCB, North China Basin; QLM, Qilian Mountain; SCB, Sichuan Basin; TLF, Tanlu fault; YC, Yangtze Craton; NCISP, North China Interior Structure Project.

Craton to the south by the E–W trending Triassic Qinling–Dabie Orogen. Integrated interpretations of the geology (Lin & Wang 2006), geochemistry (e.g. Menzies *et al.* 1993; Xu *et al.* 2004; Wu *et al.* 2005; Yang *et al.* 2008) and geophysics (e.g. Zhao & Zheng 2005; Chen *et al.* 2008; Zhao *et al.* 2009; Zhu & Zheng 2009) of this region suggest that the eastern and central North China Craton underwent significant reactivation during the Late Mesozoic and Cenozoic eras, whereas the western region remained relatively stable. In support of this interpretation, recent tomographic studies (e.g. Huang & Zhao 2006; Li *et al.* 2008; Zhao, Allen & Zheng 2011, in preparation) have shown high-velocity anomalies beneath the Ordos and Sichuan basins of the western North China Craton and Yangtze Cratons that extend to depths greater than 250 km. In contrast, the eastern North China Craton and southeast China overly lithosphere that has a thickness of less 100 km in some areas (e.g. Sodoudi *et al.* 2006; Chen *et al.* 2008). If the subcrustal impact of the India–Eurasia collision extends into North China, the central and eastern North China Craton are likely conduits for mantle flow (Fig. 1). This study analyses seismic parameters of the Qilian Mountain and the North China Craton to study mantle structure and determine whether it is impacted by the India–Eurasia collision.

Seismic mapping of anisotropic properties caused by lattice-preferred orientation of mantle minerals (mainly composed of Olivine) is a robust and informative technique for studying mantle flow (e.g. Vinnik *et al.* 1989; Silver 1996; Barruol *et al.* 1997; Karato *et al.* 2008). Laboratory studies have shown that under dry conditions and moderate-to-intense strain, the *a*-axes of olivine crystals become aligned with the direction of mantle flow (Zhang & Karato 1995). Previous studies have used *SKS* wave splitting analysis to investigate upper-mantle anisotropy beneath different regions of the North China Craton and adjacent areas (Iidaka & Niu 2001; Luo *et al.* 2004; Zhao & Zheng 2005, 2007; Chang *et al.* 2008, 2009; Huang *et al.* 2008; Liu *et al.* 2008; Wang *et al.* 2008; Zhao *et al.* 2008a; Ma *et al.* 2010; Zhao & Xue 2010). Zhao & Zheng (2005) initially observed upper-mantle anisotropy in areas beneath the eastern and central North China Craton. Huang *et al.* (2008) and Ma *et al.* (2010) developed a geodynamic model relating the western and southwestern North China Craton to the India–Eurasia

collision. Zhao & Xue (2010) incorporated forces related to the subduction of the Pacific Plate in their hybrid model for upper-mantle deformation in central and east portions of the North China Craton.

The absence of adequate seismic station coverage especially in areas bordering the North China Craton boundaries, and for the intervening region between the North China Craton and Tibet, poses a significant challenge in discerning the relative roles of Pacific Plate subduction and the India–Eurasia collision in upper-mantle deformation beneath North China (Zhao & Xue 2010). In recent years, large-scale portable seismic arrays and upgrades in the Chinese National Seismic Network (CNSN) have significantly improved the quality and extent of seismic observation in China (e.g. Zhu & Zheng 2009; Zheng *et al.* 2010). In this study, we took advantage of enhanced station coverage throughout Qilian Mountain and the North China Craton (Fig. 1). The higher resolution seismic data on which our study is based, allowed us to investigate upper-mantle anisotropy in North China and the Qilian Mountain as well as the larger scale mechanisms that may be causing upper-mantle deformation.

2 DATA AND SHEAR WAVE SPLITTING ANALYSIS

This study used data from two seismic networks, the North China Interior Structure Project (NCISP-7; 61 stations), and the CNSN (238 stations; Fig. 1). The NCISP-7 network is a dense N–S trending linear array with average station spacings of 15–20 km. NCISP-7 operated from 2008 June to 2009 August using CMG-3ESP or 3T sensors and REFTEK-72A or 130 data-acquisition systems. Data from CNSN permanent stations (red triangles in Fig. 1) were acquired from 2007 July to 2010 May (Zheng *et al.* 2010). Although data from some CNSN stations, included in our array, have been reported in previous studies (Zhao & Zheng 2005; Chang *et al.* 2008a; Ma *et al.* 2010), our study is based mainly on previously unreported data. Data collected from stations located on the Qilian Mountain and presented in a recently published paper by Li *et al.* (2011, after we had begun this work) are also reported here for the sake of consistency. Shear wave analysis was performed on a total of 67 teleseismic events occurring at distances of 85°–115° from the study area (Fig. 2). Most of these events originated in the area

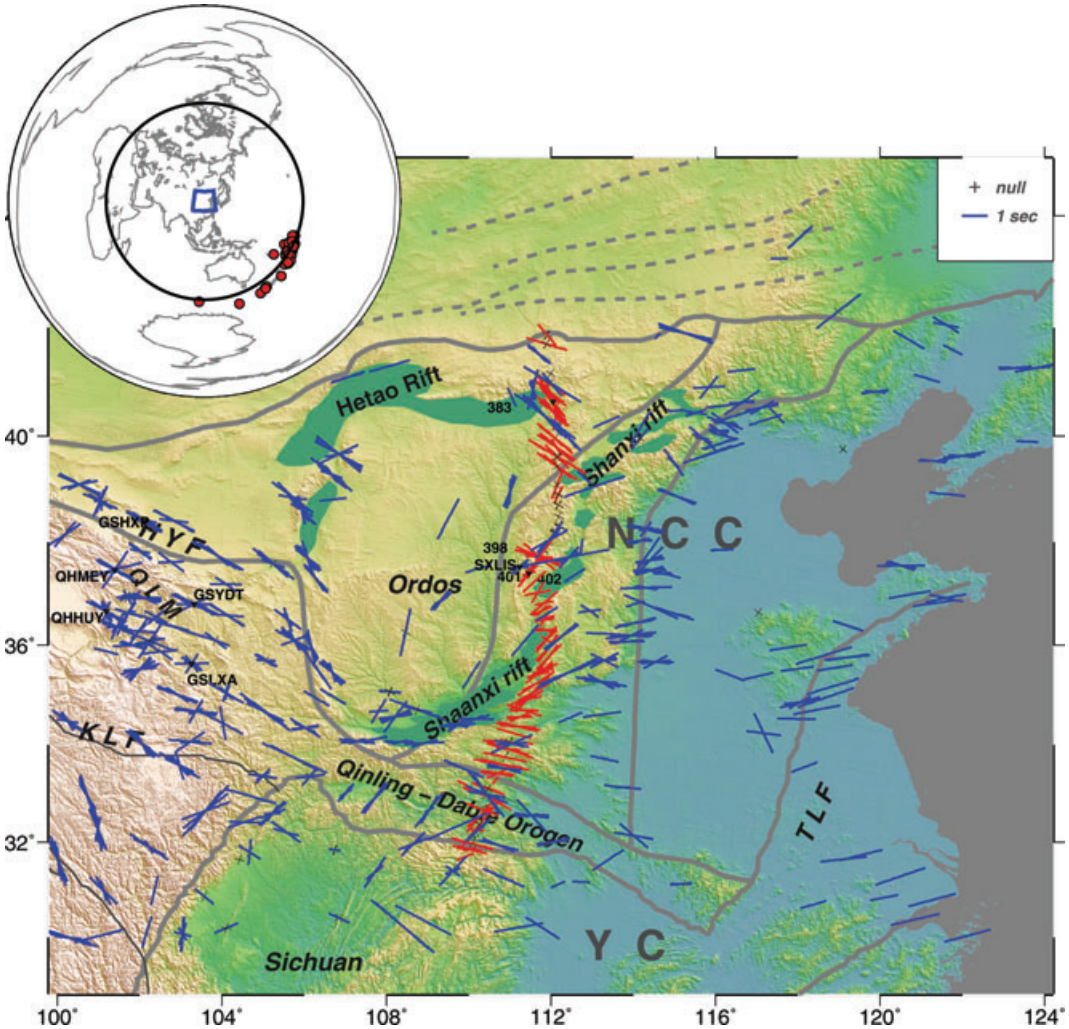

Figure 2. Map showing splitting parameters for the study region. Red bars represent results from NCISP stations and blue bars represent results from CNSN stations. The orientation of the bar indicates the fast direction and bar length is proportional to the delay time. The small grey crosses represent null results indicating shear wave orientation parallel or perpendicular to the polarization direction of the incoming waveform (the backazimuth of event). Stations mentioned in the text are marked as triangles with abbreviated labels (Table S1). The inset shows the study area (blue trapezoids) and locations of seismic events (red dots) analysed in this study.

© 2011 The Authors, *GJI*, **187,** 1027–1037
Geophysical Journal International © 2011 RAS

of the Tonga trench, or roughly, the 90°–180° quadrant of the great circle shown in the inset of Fig. 2. The majority of events are located in one quadrant (90°–180°) and mainly originated in the Tonga–Fiji zones.

SKS wave analysis followed methods of Silver & Chan (1991, called 'SC method' hereafter) which assume shear wave splitting across a single homogeneous anisotropic medium to derive the fast polarization direction (ϕ) and the delay time (δt) between the fast and slow components of the polarized *SKS* waves. Splitting parameter calculations are sensitive to the selection of the time-window from which waveforms are processed. To select the optimal time-window, we applied an auto-adapted time-windowing technique similar to that of Evans *et al.* (2006). This method begins with an initial time-window selected by visual inspection. The time-window is then adjusted to minimize errors in significance testing of the associated splitting parameters (F-test analysis; Silver & Chan 1991). As a means of quality control, we calculated signal-to-noise ratios of the radial component (SNR_r) for each *SKS* record, as the peak amplitude of a *SKS* phase versus the average amplitude of the time-window 8 s before the onset of the *SKS* phase. All *SKS* records with $SNR_r < 10$ were excluded from further analysis.

To investigate the frequency dependence of the results, we applied various two-pole Butterworth bandpass filters to the data. All the filters adopted had a fixed lower corner frequency of 0.02 Hz and varying upper corner frequencies ranging from 0.2 to 1.0 Hz. These filtering processes yielded approximately the same splitting parameters. This indicates that high-frequency scattering did not significantly affect the results.

3 SPLITTING RESULTS

Using the methods above, we obtained 1125 shear wave splitting measurements (Fig. 2; Table S1). Examples of splitting parameters for stations 383, 401, GSHXP and SXLIS (Fig. S1) show distinct variations in the transverse components of *SKS* waveforms and splitting parameters. Fig. 2 shows splitting parameters for the entire study area. The fast directions exhibit complex patterns on a regional scale but are relatively coherent within individual tectonic blocks. We describe salient features of fast direction patterns below.

(1) Fast directions are parallel to the strike of the entire southern boundary zone of the North China Craton, extending from 100 °E to 116 °E longitude. These results are consistent with previous regional studies of the western and the southwestern boundaries of the North China Craton (Huang *et al.* 2008; Ma *et al.* 2010).

(2) Ten stations located within the Qinling–Dabie Orogen and near the northern boundary of the Yangtze Craton yielded NE–SW trending fast directions, which contrasted fast directions given by adjacent stations to the south and north. The NE–SW fast directions are parallel to the structural orientations of the local extensional basins within the Qinling–Dabie Orogen. The distance separating stations where contrasting fast directions were observed was less than 100 km. The variation in splitting parameters from these relatively closely spaced stations may be due to the complex upper-mantle anisotropy beneath this region.

(3) Stations within the Qilian Mountain (the intervening region between the Haiyuan and Kunlun faults) yielded splitting parameters that varied significantly with the backazimuths of given events (see Fig. 3). These results are consistent with those of a similar study by Li *et al.* (2011) which analysed *PKS* and *SKKS* phases in addition to *SKS* phases. Backazimuth dependence of fast directions indicates complexity in the mantle structure beneath these stations, such as a multilayer anisotropy (Li *et al.* 2011) or anisotropy with a dipping symmetry axis (see discussion in Section 5.2).

(4) Along the southern segment of the NCISP-7 network and the Shaanxi rift, fast directions trend mostly in E–W to ESE–WNW directions with average delay times of 1.1 s. These results are consistent with previous findings concerning the nearby Shaanxi rift system (Huang *et al.* 2008; Zhao & Xue 2010). Fast directions change dramatically from south to north along the central segment of the NCISP-7 network, rotating from E–W to NE–SW. Further north, fast directions change dramatically from NE–SW to NW–SE (stations 402–398; Fig. 2). Station coverage is dense in this segment of the network, with less than 40 km distance between stations reporting the greatest change in fast directions. Along the most northerly segment of the NCISP-7 network, near the Shanxi rift, the fast directions are uniform with a NW–SE orientation. Delay times from this segment are more variable however, ranging from 0.5 s to more than 2.0 s. These results are in good agreement with those of a previous study by Zhao *et al.* (2008a).

(5) Fewer splitting parameters were available from stations located along the Tanlu fault zone and within the eastern Yangtze Craton. The available fast directions were consistently oriented from E–W to ENE–SWS, with delay times ranging from 1.0 to 1.6 s. These results are consistent with those of previous studies performed over a larger area (Zhao *et al.* 2007; Zheng *et al.* 2008b).

4 DEPTH OF ORIGIN OF THE ANISOTROPY

4.1 Crustal contribution

In the North China Craton, the measurements of shear wave splitting in crust show that the average normalized slow wave time delay is 3.55 ± 2.93 ms km^{-1} (Wu *et al.* 2009). Assuming an average crustal shear wave velocity of 3.6 km s^{-1}, this range of delay time corresponds to 0.2–2.3 per cent anisotropy. With a crustal thickness of 30–45 km in the North China Craton (Zheng *et al.* 2008a; Zhu & Zheng 2009), the predicted maximum delay time for a 45-km-thick crust is ∼0.25 s. Based on comparison with the majority of measured delay times, which range from 0.8 to 2.0 s, the upper mantle appears to be the primary source of the observed seismic anisotropy.

4.2 Test of a simple asthenospheric flow model

To investigate the contribution from asthenospheric flow, we compare the fast direction with the absolute plate motion (APM). If a plate couples with the underlying asthenosphere, the plate motion directions should indicate the motion of asthenospheric flow. The hotspot frame HS3-NUVEL1a model (Gripp & Gordon 2002) predicts a coherent APM direction of ∼N287° ± 5° in the study area, which does not match the observed spatial change of fast directions. This means a simple uniform mantle convection model is incompatible with the complex-splitting observations in the study area.

4.3 Contributions from lithosphere and/or asthenosphere

Fig. 4 shows shear wave analysis results from this study along with data from previous studies (Iidaka & Niu 2001; Luo *et al.* 2004; Zhao & Zheng 2005, 2007; Huang *et al.* 2008; Liu *et al.* 2008; Zhao *et al.* 2008a; Zhao & Xue 2010), overlaid on a current

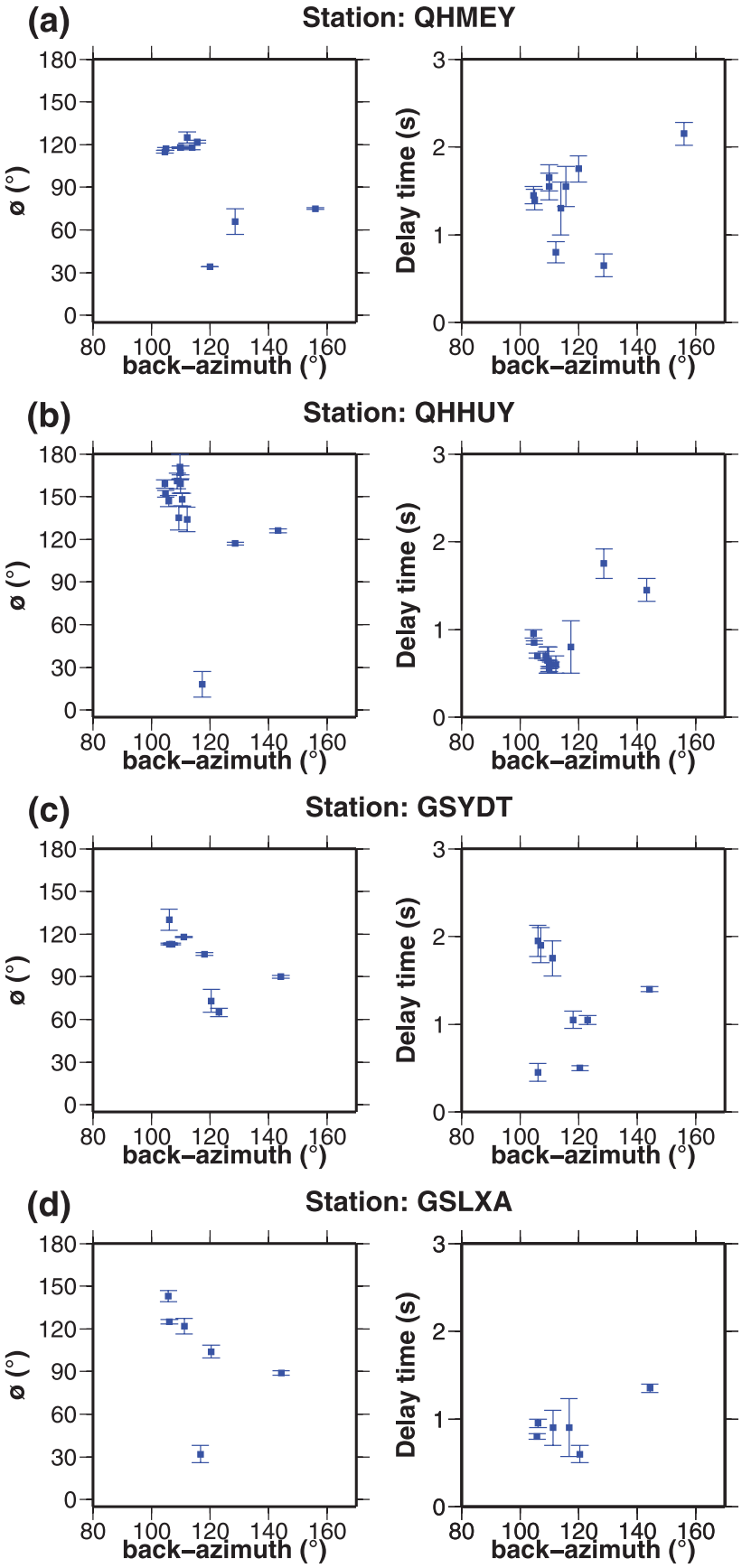

Figure 3. Relationship between splitting parameters (the fast polarization direction ϕ, shown left and the delay time δt, shown right) versus backazimuth for four stations located in the Qilian Mountain area (station locations labelled in Fig. 2). The rectangle indicates the parameter value; thin bars represent 2σ error.

© 2011 The Authors, *GJI*, **187,** 1027–1037
Geophysical Journal International © 2011 RAS

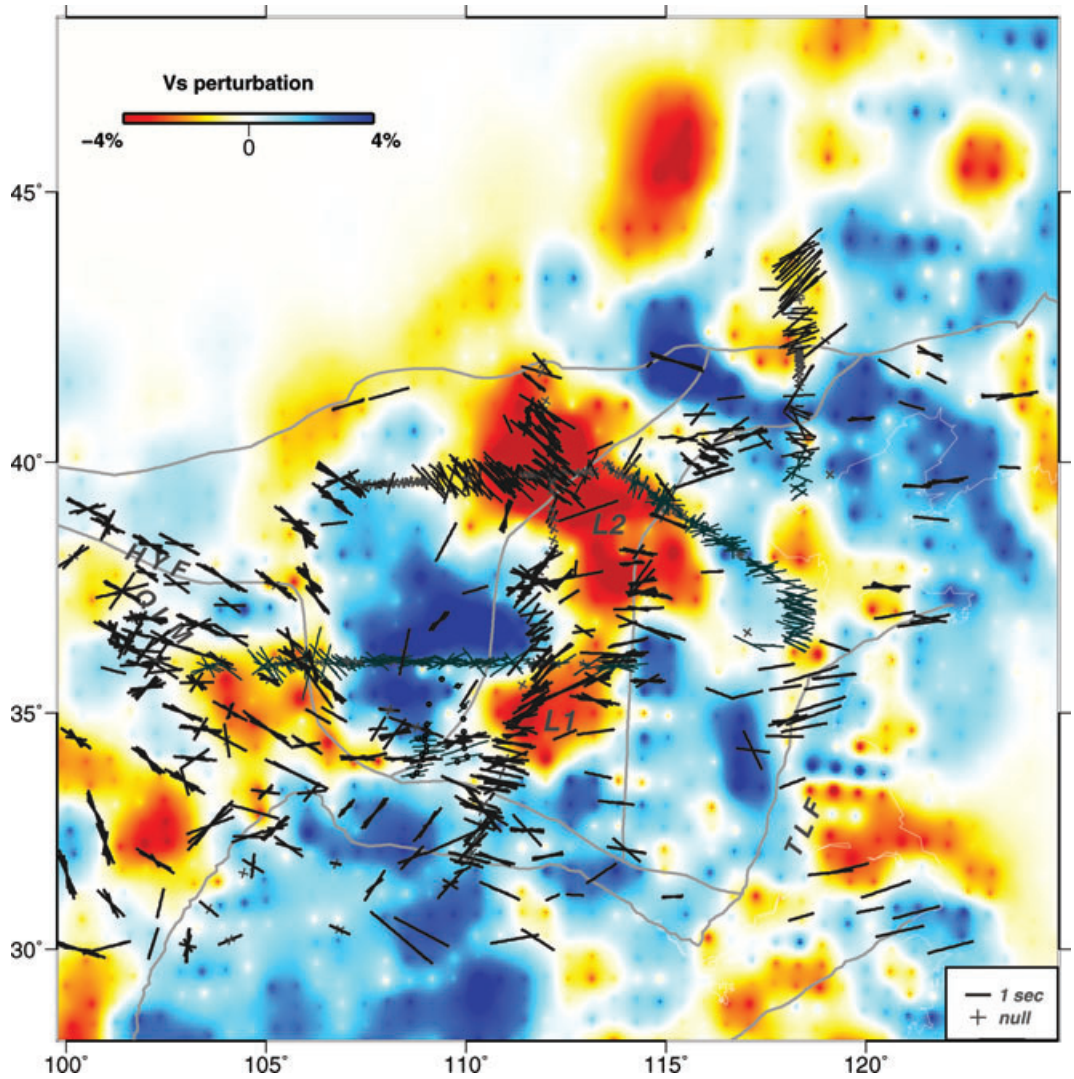

Figure 4. Splitting measurements obtained by this study (thick bars) and from previous studies (thin bars) overlaid on a tomographic image of the region (shear wave velocity vertically averaged over 100–300 km depth; Zhao *et al.* in preparation). Thin grey bars are results from Zhao & Zheng (2005, 2007), Zhao *et al.* (2008) and Zhao & Xue (2010); thin bars with circles are from Iidaka & Niu (2001), Luo *et al.* (2004), Huang *et al.* (2008) and Liu *et al.* (2008). The colour-scale bar represents the degree of shear wave velocity variation.

shear wave tomographic model of the region (Zhao *et al.* 2009, in preparation). The tomographic image is normalized to the vertical average of the shear wave velocity calculated from 100 to 300 km depth, the range over which most interactions between the asthenosphere and lithosphere generally occur. Shear wave velocity anomalies can arise in the upper mantle from both temperature differences and partial melting (e.g. Cammarano *et al.* 2003). Theoretical models predict that a 2.5 per cent anomaly corresponds to ∼200 °C temperature perturbation for dry conditions, at 200 km depth. We assume the variation in velocity anomalies observed in our data reflects the spatial distribution of the lithosphere and asthenosphere.

Regional patterns in splitting parameters are remarkably consistent with shear wave velocity anomalies (Fig. 4). The fast directions along boundaries of the L1 and L2 low-velocity zones, for example, rotate in accordance with surrounding high-velocity anomalous volumes (colder zones). The correspondence between shear wave velocity perturbations and the orientation of anisotropy suggests that anisotropy is due to vertically impinging non-lithospheric mantle material beneath the areas with thin lithospheric roots. The thickness of the lithospheric beneath L1 and L2 zones is probably around 80 km, assuming a 30–42-km-thick crust (Zheng *et al.* 2009; Zhu & Zheng 2009), and a lithospheric mantle thickness of about 40–50 km. An 80-km-thick lithosphere with 4 per cent anisotropy would generate shear wave splitting delay times of 0.4–0.5 s. The majority of delay times observed from stations located on the central North China Craton are greater than 1.0 s, and many reach durations of ∼1.5 s (Table S1). This indicates that the non-lithospheric mantle contributes to the observed anisotropy. For areas having substantially thicker lithospheric roots (>150 km), such as the Ordos and Yangtze cratons, the lithosphere alone can account for all of the observed anisotropic properties.

5 DISCUSSION

In this section, we discuss what our findings suggest about the extent to which the India–Eurasia collision has affected upper-mantle deformation beneath the North China Craton and the Qilian Mountain.

5.1 The dynamic effect of the India–Eurasia collision in the Qilian Mountain

The fast directions along the entire southern boundary of the North China Craton coincide well with the dominant structural grain of the area (Fig. 2). *SKS* splitting parameters from orogenic belts usually exhibit fast directions polarized parallel to the trend of mountain ranges, faults and other tectonic features (e.g. Nicolas 1993). Fast direction trends from our study indicate that development of upper-mantle anisotropy accompanied E–W trending Qinling–Dabie orogenic events and WNW–ESE trending Qilian Mountain orogenic events.

Teleseismic results from the Qilian Mountain, however, require more detailed analysis and interpretation. Similar to results described above, Li *et al.* (2011) reported dependence of splitting parameters on backazimuths, and proposed a two-layer anisotropy model for the area between the Haiyuan and Kunlun faults. Tomographic imaging of the Qilian Mountain indicates that the lithosphere becomes progressively thicker from the Qilian Mountain to the Ordos basin, which may contribute to anisotropy with a dipping axis of symmetry.

To examine the theoretical implications of a double-layer anisotropy with a dipping symmetry axis, we modelled wave propagation in this type of localized heterogeneous anisotropic media, using 2-D synthetic seismograms (Zhao *et al.* 2008b). We specifically calculated *SKS* waveforms for (a) an anisotropic lithosphere overlying an anisotropic asthenosphere and (b) one slab of lithosphere overriding another, for example, a lithospheric slab being underplated by collisional tectonics (Silver & Savage 1994). We assumed a thickness of 60 km for the overlying layer and fixed its fast polarization direction to 90°N. The underlying or underplated layer was also assumed to be 60 km thick, but with a fast direction of 135° N. The underlying layer was given a downward-dipping symmetry axis of 30° (Fig. 5a). We then generated radial and transverse seismic waveforms by changing the incoming *SKS* energy polarization direction from north to south, in increments of 10° (Fig. 5b). We defined the radial and transverse axes as parallel and perpendicular to the incoming *SKS* energy direction, respectively. A bandpass filter of 0.02–0.30 Hz was applied to the synthetic waveforms, which were then processed for theoretical splitting parameters.

The apparent splitting parameters calculated by the SC method appear to be functions of incoming polarization direction with a period of approximately $\pi/2$. Fig. 5(c) shows an abrupt change in synthetic splitting parameters similar to that observed for splitting parameters from the Qilian Mountain. The observed dependence between splitting parameters and the backazimuths suggests a multilayer anisotropy with a dipping symmetry axis. Unfortunately, the splitting parameters available from the study area do not allow us to investigate anisotropic features in greater detail.

If mantle flow (or a local flow cell) from the India–Eurasia collision has reached areas beneath the Qilian Mountain, obstruction by the thicker lithosphere beneath the Ordos Craton could create the multilayer and/or dipping symmetry axis anisotropy observed from splitting parameters. The tectonic history in this region indeed suggests that the multilayer or/and dipping axis anisotropy could be a regional shearing effect caused by the India–Eurasia collision.

5.2 The effects of the India–Eurasia collision on mantle flow beneath the Qinling–Dabie Orogen

Mantle flow patterns beneath the Tibet Plateau are poorly constrained due to the incomplete understanding of upper-mantle thermal structure, and lack of high-resolution images of the lithosphere–asthenosphere boundary (LAB). If mantle flow beneath the central North China Craton is directly impacted by the India–Eurasia collision, upper-mantle deformation and asthenospheric flow should exhibit a consistent and continuous pattern from northeastern Tibet to the North China Craton.

Results of this study, however, indicate that eastward mantle flow is not channelled beneath the Qinling–Dabie Orogen. The splitting parameters in the Qinling–Dabie Orogen do not exhibit the expected continuous spatial patterns. High-velocity anomalies (V_P and V_S) for this region extend to >200 km depths, implying a cold and stationary lithosphere rather than an active asthenospheric channel. Potential mantle flow would be blocked by the thicker eastern portions of lithosphere observed beneath the western North China Craton and the Yangtze Craton. Signs of deflected mantle flow associated with this obstacle are absent. The abrupt variation of fast directions in the southern Qinling–Dabie Orogen may instead reflect vestigial anisotropy that developed during the amalgamation of the Yangtze Craton and the North China Craton, or during subsequent regional extensional events (Meng & Zhang 2000; Faure *et al.* 2008). Detailed study of the larger tectonic framework of the region, especially the south China block could further elucidate the causes of anisotropy observed beneath the southern Qinling–Dabie Orogen, but these efforts are beyond the scope of this study.

5.3 Cause of the mantle flow beneath the central North China Craton

Fast directions from stations located along the Shaanxi–Shanxi rift systems in the central North China Craton are strongly correlated with velocity anomalies in the upper mantle. Given the relatively thin lithosphere of this region (<100 km; Chen *et al.* 2008), we interpret the anisotropy as an asthenospheric feature. Tomographic imaging of the North China Craton (Zhao *et al.* 2009, in preparation) shows that low-velocity anomalies L1 and L2, might stem from the mantle transition zone. Recent studies of seismic receiver functions also support the existence of upward asthenospheric flows arising from the mantle transition zone or regions deeper (e.g. Xu *et al.* 2011). Together, these lines of evidence indicate that a regional upwelling cell, with no direct relation to the India–Eurasia collision may cause upper-mantle deformation beneath the central North China Craton.

A regional upwelling cell would be expected to generate anisotropy with a vertical axis of symmetry from the vertical column of asthenospheric flow. Shear wave splitting should not be observed under these circumstances, because the axis of symmetry for the anisotropic zone would be parallel to the vertically propagating *SKS* waves. Splitting parameters for the central North China Craton, however, were robustly detected with fast directions parallel to the strike of the local rift systems. Irregularities in the LAB can modify asthenospheric flow (Bormann *et al.* 1996), and we suggest that this mechanism may be operating in the central North China Craton. Vertical columns rising from the mantle transition zone are deflected when they encounter resistance at the LAB. The coherent spatial variation of the fast directions and the low-velocity anomalous volumes for the North China Craton imply that deflected asthenospheric flow has rotated of the symmetry axis of anisotropy.

On a regional scale, the westward thickening LAB will also affect the horizontally deflected asthenospheric flow, generating an anisotropic pattern aligned with the LAB topography (Fig. 6). The largest delay time (δt) values were observed from stations located

© 2011 The Authors, *GJI*, **187,** 1027–1037
Geophysical Journal International © 2011 RAS

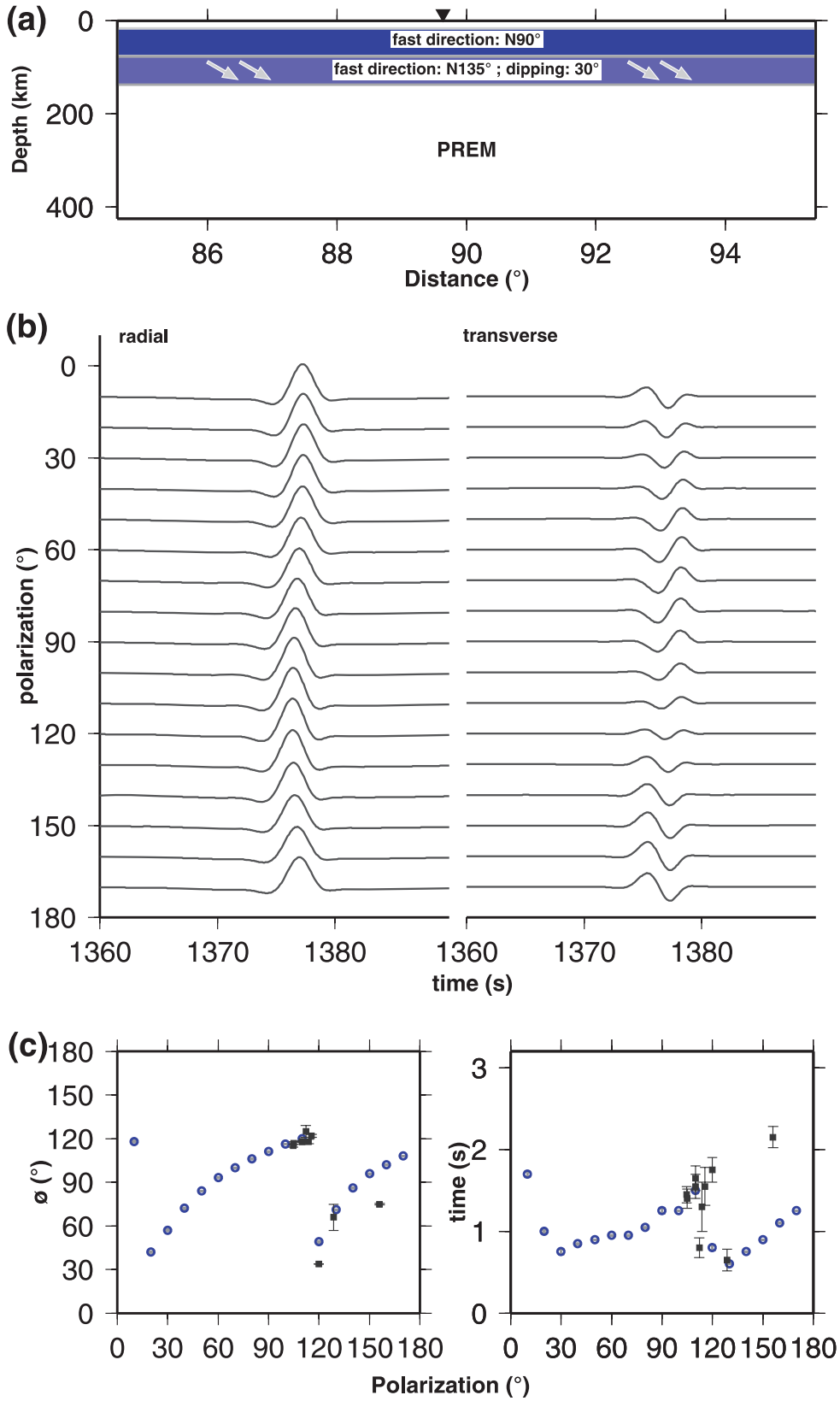

Figure 5. Experimental model of shear wave splitting parameters for an area with two anisotropic layers. (a) The fast direction of anisotropy for the overlying layer trends at 90° N, whereas that of the underlying layer trends at 135° N. The axis of symmetry for the anisotropy (underlying layer) dips at 30°. The triangle represents the location of the receiver from which theoretical 2-D seismograms are calculated. (b) Waveforms for incoming *SKS* phases polarized by the multilayer anomaly shown in (a). The vertical axis represents the polarization direction. Synthetic waveforms were subject to a 0.02 and 0.30 Hz bandpass filter. (c) Splitting parameters ϕ (left) and δt (right) from the calculated waveforms (blue circles) and observed splitting parameters from station QHMEY (black squares). Thin bars represent 2σ error.

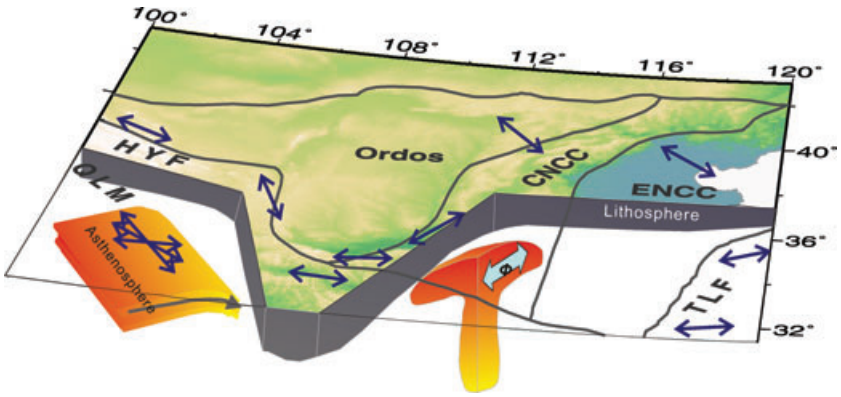

Figure 6. Schematic diagram showing a regional interpretation of splitting parameter results. Bidirectional arrows show the general fast directions of given regions. A multilayer anisotropy and/or anisotropy with a dipping symmetry axis is shown beneath the Qilian Mountain. Deflected flow from asthenospheric upwelling is shown beneath the central North China Craton.

within the L2 zone of the central North China Craton. Tomographic models for this area show that $\partial \ln V_S / \partial \ln V_P$ parameters reach values greater than 2.2 beneath the L2 zone (Zhao *et al.* in preparation). Velocity models inferred from temperature data give a $\partial \ln V_S / \partial \ln V_P$ range of 1.3–2.2 (from low to high temperatures) for the upper mantle (Cammarano *et al.* 2003). Partial melting of the upper mantle would cause higher $\partial \ln V_S / \partial \ln V_P$ values of ∼2.2–2.3 (Hammond & Humphreys 2000; Schmandt & Humphreys 2010). Larger than expected δt values observed from the L2 zone thus indicate that anisotropy is enhanced by vertically aligned melt-filled cracks (e.g., Wolfe & Solomon 1998). The nearby Shaanxi–Shanxi rift and Hetao rift systems are coupled to upper-mantle deformation and offer a regional tectonic context for deflected upwelling and partial melting mechanisms described earlier.

6 CONCLUSIONS

We calculated *SKS* wave splitting parameters derived from teleseismic events recorded by 299 stations throughout eastern China. We obtained 1125 splitting parameters that provided excellent regional coverage for investigating upper-mantle deformation beneath the North China Craton and the Qilian Mountain.

Splitting parameters from the study revealed subsurface patterns that could not be explained by simple asthenospheric flow. Shear wave fast directions varied in accordance with shear wave velocity anomalies. The consistency between these two parameters in regions with thin lithosphere (<100 km) indicates that anisotropy has developed primarily in the non-lithospheric mantle. In areas with thicker lithospheric roots (>150 km), such as the Ordos and Yangtze cratons, anisotropy has developed in the lithosphere as well as the asthenosphere. For areas like the Shanxi rift system, $\partial \ln V_S / \partial \ln V_P$ reached values of up to 2.2 for the upper mantle. Velocity variations of this magnitude, along with larger than expected delay times indicate that vertically aligned, melt-filled cracks contribute to the anisotropy beneath these regions.

Splitting parameters from the Qilian Mountain exhibited strong backazimuth dependence. Literature sources and theoretical modelling suggest that multilayer anisotropy and/or anisotropy with a dipping symmetry axis can cause the observed dependence. The complex structure of the lithosphere, and mantle flow beneath the southwest boundary of the North China Craton thus show some effects of the long-range impact of the India–Eurasia collision. These effects, however, are limited to subsurface dynamics beneath the Qilian Mountain.

In contrast, the upper-mantle anisotropy beneath the central North China Craton is not caused by the India–Eurasia collision, but instead may originate from regional asthenospheric upwelling. We observed strong anisotropy in this area that may result from mantle flow that is horizontally deflected by the thickened lithospheric roots of the North China Craton.

ACKNOWLEDGMENTS

Waveform data are provided by Seismological Laboratory, IGGCAS and Data Management Centre of China National Seismic Network at Institute of Geophysics, China Earthquake Administration. We thank editor Jeannot Trampert and two anonymous reviewers for their constructive reviews. This research was financially supported by the NSFC Grant 90914011, 90814002 and 40974030.

REFERENCES

Barruol, G., Silver, P.G. & Vauchez, A., 1997. Seismic anisotropy in the eastern US: deep structure of a complex continental plate, *J. geophys. Res.,* **102,** 8329–8348.

Bormann, P., Grünthal, G., Kind, R. & Montag, H., 1996. Upper mantle anisotropy beneath Central Europe from SKS wave splitting: effects of absolute plate motion and lithosphere–asthenosphere boundary topography, *J. Geodyn.,* **22,** 11–32.

Cammarano, F., Goes, S., Vacher, P. & Giardini D., 2003. Inferring upper-mantle temperatures from seismic velocity, *Phys. Earth planet. Inter.,* **138,** 197–222.

Chang, L., Wang, C. & Ding, Z., 2008. (in Chinese with English abstract) A study on SKS splitting beneath capital area of China, *Acta Seismol. Sin.,* **30,** 551–559.

Chang, L., Wang, C. & Ding, Z., 2009. Seismic anisotropy of upper mantle in eastern China, *Sci. China Ser. D-Earth Sci.,* **52,** 774–783.

Chen, L., Wang, T., Zhao, L. & Zheng T., 2008. Distinct lateral variation of lithospheric thickness in the Northeastern NCC, *Earth planet. Sci. Lett.,* **267,** 56–68.

Duvall, A.R. & Clark, M.K., 2010. Dissipation of fast strike-slip faulting within and beyond northeastern Tibet, *Geology,* **38,** 223–226.

Evans, M.S., Kendall, J. M. & Willemann, R.J., 2006. Automated SKS splitting and upper-mantle anisotropy beneath Canadian seismic stations, *Geophys. J. Int.,* **165,** 931–942.

Faure, M., Lin, W., Monié, P. & Meffre, S., 2008. Palaeozoic collision between the North and South China blocks, Triassic intracontinental tectonics, and the problem of the ultra-pressure metamorphism, *C.R. Geosci.,* **340,** 139–150.

Gripp, A.E. & Gordon, R.G., 2002. Young tracks of hotspots and current plate velocities, *Geophys. J. Int.,* **150,** 321–361.

Hammond, W.C. & Humphreys, E.D., 2000. Upper mantle seismic wave velocity: effects of realistic partial melt geometries, *J. geophys. Res.,* **105,** 10 975–10 986.

Huang, J. & Zhao, D., 2006. High-resolution mantle tomography of China and Surrounding regions, *J. geophys. Res.,* **111,** B09305, doi:10.1029/2005JB004066.

Huang, Z., Xu, M., Wang, L., Mi, N., Yu, D. & Li, H., 2008. Shear wave splitting in southern margin of the Ordos Block, north China, *Geophys. Res. Lett.,* **35,** L19301, doi:10.1029/2008GL035188.

Iidaka, T. & Niu, F.L., 2001. Mantle and crust anisotropy in the eastern China region inferred from waveform splitting of SKS and PpSms, *Earth Planet. Space,* **53,** 159–168.

Karato, S., Jung, H., Katayama, I. & Skemer P., 2008. Geodynamic significance of seismic anisotrophy: New insights from laboratory studies, *Ann. Rev. Earth Planet. Sci.,* **36,** 59–95.

Kind, R. & Yuan, X.H., 2010. Seismic images of the biggest crash on Earth, *Science,* **327,** 1479–1480.

Li, C., Van der Hilst, R.D., Meltzer, A. & Engdahl E.R., 2008. Subduction of the Indian lithosphere beneath the Tibetan Plateau and Burma, *Earth planet. Sci. Lett.,* **274,** 157–168.

Li, Y., Wu, Q., Zhang, F., Feng, Q. & Zhang, R., 2011. Seismic anisotropy of the Northeastern Tibetan Plateau from shear wave splitting analysis, *Earth planet. Sci. Lett.,* **304,** 147–157.

Li, Z.X. & Li, X.H., 2007. Formation of the 1300 km-wide intra-continental orogen and post-orogenic magmatic province in Mesozoic South China: a flat-slab subduction model, *Geology,* **35,** 179–182.

Lin, W. & Wang, Q., 2006. Late Mesozoic extensional tectonics in the North China block: a crustal response to subcontinental mantle removal? *Bull. Soc. geol. France,* **177,** 287–297.

Liu, K.H., Gao, S., Gao, Y. & Wu, J., 2008. Shear wave splitting and mantle flow associated with the deflected Pacific slab beneath northeast Asia, *J. geophys. Res.,* **113,** B01305, doi:10.1029/2007JB005178.

Liu, M., Cui, X. & Liu, F., 2004. Cenozoic rifting and volcanism in eastern China: a mantle dynamic link to the Indo–Asian collision? *Phys. Earth planet. Inter.,* **393,** 29–42.

Luo, Y., Huang, Z.X., Peng, Y.J. & Zheng, Y.J., 2004. A study on SKS wave splitting beneath the China mainland and adjacent regions, *Chinese J. Geophys.* (in Chinese), **47,** 812–821.

Ma, H., Ding, Z., Chang, L., Gao, W. & Cai, X., 2010. Seismic anisotropy of the upper mantle in Ningxia region, *Acta Seismol. Sin.,* **32,** 507–516.

Meng, Q.R. & Zhang, G.W., 2000. Geologic framework and tectonic evolution of the Qinling orogen, central China, *Tectonophysics,* **323,** 183–196.

Menzies, M.A., Fan, W. & Zhang, M., 1993. Palaeozoic andCenozoic lithoprobes and the loss of N120 km of Archean lithosphere, Sino-Korean craton, China, in *Magmatic Processes and Plate Tectonics,* pp. 71–81, eds Prichard, H.M., Alabaster, T., Harris, N.B.W. & Neary C.R., Spec. Publ. 76, Geol. Soc. London.

Molnar, P. & Tapponnier, P., 1975. Cenozoic tectonics of Asia: effects of a continental collision, *Science,* **189,** 419–426.

Nicolas, A., 1993. Why fast polarization directions of SKS seismic waves are parallel to mountain belts, *Phys. Earth planet. Inter.,* **78,** 337–342.

Niu, Y.L., 2005. Generation and evolution of basaltic magmas: some basic concepts and a new view on the origin of Mesozoic-Cenozoic basaltic volcanism in eastern China, *Geol. J. China Univ.,* **11,** 9–46.

Royden, L.H., Burchfier, B.C. & van der Hilst, R.D., 2008. The geological evolution of the Tibetan Plateau, *Science,* 1054–1058.

Schmandt, B. & Humphreys, E., 2010. Complex subduction and small-scale convection revealed by body-wave tomography of the western United States upper mantle, *Earth planet. Sci. Lett.,* **297,** 435–445.

Silver, P.G., 1996. Seismic anisotrophy beneath the continents: Probing the depths of geology, *Ann. Rev. Earth Planet. Res.,* **24,** 385–432.

Silver, P.G. & Chan, W.W., 1991. Shear wave splitting and subcontinental mantle deformation, *J. geophys. Res.,* **96,** 16 429–16 454.

Silver, P.G. & Savage, M.K., 1994. The interpretation of shear-wave splitting parameters in the presence of two anisotropic layers, *Geophys. J. Int.,* **119,** 949–963.

Sodoudi, F., Yuan, X., Liu, Q., Kind, R. & Chen, J., 2006. Lithospheric thickness beneath the Dabie Shan, central eastern China from S receiver functions, *Geophys. J. Int.,* **166,** 1363–1367.

Tang, Y., Zhang, H. & Ying, J., 2006. Asthenosphere–lithospheric mantle interaction in an extensional regime: implication from the geochemistry of Cenozoic basalts from Taihang Mountains NCC, *Chem. Geol.,* **233,** 309–327.

Tapponnier, P. Z., Xu, Q., Roger, F., Meyer, B., Arnaud, N., Wittlinger, G. & Yang, J., 2001. Oblique stepwise rise and growth of the Tibet Plateau, *Science,* **294,** 1671–1677.

Vinnik, L.P., Farra, V. & Romanowicz, B., 1989. Azimuthal anisotrophy in the earth from observations of SKS at SCOPE and NARS broadband stations, *Bull. seism. Soc. Am.,* **79,** 1542–1558.

Wang, C.Y., Zhang, Q., Quan, Q. & Zhou, M.F., 2005. Geochemistry of the Early Paleozoic Baiyin Volcanic Rocks (NW China): implications for the Tectonic Evolution of the North Qilian Orogenic Belt, *J. Geol.,* **113,** 83–94.

Wang, C-Y., Flesch, L.M., Silver, P.G., Chang, L-J & Chan, W.W., 2008. Evidence for mechanically coupled lithosphere in central Asia and resulting implications, *Geology,* **36,** 363–366.

Wolfe, C.J. & Solomon, S.C., 1998. Shear-wave splitting and implications for mantle flow beneath the MELT region of the East Pacific Rise, *Science,* **280,** 1230–1232.

Wu, F.Y., Lin, J.Q., Wilde, S.A., Zhang, X.O. & Yang, J.H., 2005. Nature and significance of the Early Cretaceous giant igneous event in eastern China, *Earth planet. Sci. Lett.,* **233,** 103–119.

Wu, J., Gao, Y. & Chen, Y.T., 2009. Shear-wave splitting in the crust beneath the southeast Capital area of North China, *J. Seismol.,* **13,** 277–286.

Xu, W.W., Zheng, T.Y. & Zhao, L., 2011. Mantle dynamics of the reactivating NCC: constraints from the topographies of the 410 km and 660 km discontinuities, *Sci. China (Ser. D)*.

Xu, Y.G., Chung, S.L., Ma, J.L. & Shi, L.B., 2004. Contrasting Cenozoic lithospheric evolution and architecture in the western and eastern Sino-Korean craton: constraints from geochemistry of basalts and mantle xenoliths, *J. Geol.,* **112,** 593–605.

Yang, J.H., Wu, F.Y., Wilde, S.A., Belousova, E. & Griffin, W.L., 2008. Mesozoic decratonization of the North China block, *Geology,* **36,** 467–470.

Ye, H., Zhang, B. & Mao, F., 1987. The Cenozoic tectonic evolution of the Great North China: two types of rifting and crustal necking in the Great North China and their tectonic implications, *Tectonophysics,* **133,** 217–227.

Zhang, S.Q. & Karato, S.I., 1995. Lattice preferred orientation of olivine aggregates deformed in simple shear, *Nature,* **375,** 774–777.

Zhang, Z.J., Yuan, X.H., Chen, Y., Tian, X.B., Kind, R., Li, X.Q. & Teng, J.W., 2010. Seismic signature of the collision between the east Tibetan escape flow and the Sichuan Basin, *Earth planet. Sci. Lett.,* **292,** 254–264.

Zhao, L. & Xue, M., 2010. Mantle flow pattern and geodynamic cause of the NCC reactivation: evidence from seismic anisotropy, *Geochem. Geophys. Geosyst.,* **11,** Q07010, doi:10.1029/2010GC003068.

Zhao, L. & Zheng, T.Y., 2005. Using shear wave splitting measurements to investigate the upper mantle anisotropy beneath the NCC: distinct variation from east to west, *Geophys. Res. Lett.,* **32,** L10309, doi: 10.1029/2005GL022585.

Zhao, L. & Zheng, T.Y., 2007.Complex upper mantle deformation beneath the NCC: implications for lithospheric thinning, *Geophy. J. Int.,* **170,** 1095–1099.

Zhao, L., Zheng, T.Y. & Lu, G., 2008a. Insight into craton evolution: constraints from shear wave splitting in the NCC, *Phys. Earth planet. Inter.,* **168,** 153–162.

Zhao, L., Wen, L.X., Chen, L. & Zheng, T.Y., 2008b. A two-dimensional hybrid method for modeling seismic wave propagation in anisotropic media, *J. geophys. Res.,* **113,** B12307, doi:10.1029/2008JB005733.

Zhao, L., Allen, R.M., Zheng, T.Y. & Hung, S., 2009. Reactivation of an Archean craton: constraints from P- and S-wave tomography in North China, *Geophys. Res. Lett.,* **36,** L17306, doi:10.1029/2009GL039781.

Zheng, T.Y., Zhao, L. & Zhu, R.X., 2008a. Insight into the geodynamics of cratonic reactivation from seismic analysis of the crust-mantle boundary, *Geophy. Res. Lett.,* **35,** L08303, doi:10.1029/2008GL033439.

Zheng, T.Y., Zhao, L., Xu, W.W. & Zhu, R.X., 2008b. Insight into modification of NCC from seismological study in the Shandong Province, *Geophy. Res. Lett.,* **35,** L22305, doi:10.1029/2008GL035661.

Zheng, T.Y., Zhao, L. & Zhu, R.X., 2009. New evidence from seismic imaging for subduction during assembly of the NCC, *Geology,* **37,** 395–398.

Zheng, X.F, Yao, Z.X., Liang, J.H. & Zheng, J., 2010. The role played and opportunities provided by IGP DMC of China National Seismic Network in Wenchuan, *Bull. seism. Soc. Am.,* **100,** 2866–2872.

Zhu, R.X. & Zheng, T.Y., 2009. Destruction geodynamics of the NCC and its Paleoproterozoic plate tectonics, *Chinese Sci. Bull.,* **54,** 1–13.

SUPPORTING INFORMATION

Additional Supporting Information may be found in the online version of this article:

Supplement. This material contains results of individual splitting measurements obtained at each station, and examples of individual shear wave splitting measurements at stations 383, 401, GSHXP and SXLIS for event 2008:245:04:00.

Please note: Wiley-Blackwell is not responsible for the content or functionality of any supporting materials supplied by the authors. Any queries (other than missing material) should be directed to the corresponding author for the article.